Refined Thomas-Fermi description of hot nuclei

J. N. De and N. Rudra*
Variable Energy Cyclotron Centre, 1/AF, Bidhannagar, Calcutta-700 064, India

Subrata Pal and S. K. Samaddar
Saha Institute of Nuclear Physics, 1/AF, Bidhannagar, Calcutta-700 064, India
(Received 26 April 1995)

Self-consistent density profiles of two-component hot nuclei in equilibrium with an external gas are calculated in the semi-classical Thomas-Fermi model with a new prescription. The energy functional is calculated with a momentum and density dependent finite range two-body effective interaction. The evolution of equilibrium nuclear masses as a function of temperature and densities of the external neutron and proton gas is investigated in this description. Limiting temperatures of nuclei, their lifetimes against neutron evaporation, temperature dependence of incompressibilites of finite nuclei and a few other observables are also studied in the present model.

PACS number(s): 21.60.−n, 21.10.−k, 21.30.Fe, 21.65.+f

I. INTRODUCTION

The properties of hot nuclear systems created in the laboratory in intermediate energy heavy ion collisions can now be investigated experimentally [1]. They give us information about the temperature dependence of the surface tension of finite nuclei, their incompressibility, level density parameter, etc., which are extremely useful in answering some important questions of astrophysical interest. The hot nuclei so created are not thermodynamically stable; they deexcite by emission of nucleons and light particles. The theoretical modeling of such an evaporating nucleus poses some problems. The continuum states of a nucleus at nonzero temperature are occupied with probability given by a Fermi factor [2] as a result of which the particle density does not vanish at large distances. The extracted observables then depend on the size of the box in which the calculation is performed. For not too high temperatures, the evaporation times are quite long; the nucleus can then be considered to be in a metastable state, very much like a superheated liquid drop [3]. A free variation of the density profiles in the Thomas-Fermi (TF) description can then lead to a solution of the density in a sphere of radius R (which is also given variationally) with zero pressure outside, but with externally given boundary conditions; i.e., the derivatives of the density at the center and at the surface should be zero [4]. In earlier thermal Hartree-Fock (HF) [5] or semiclassical calculations [6,7], this problem was circumvented either by imposing artificial conditions on the size of the basis states or by demanding an exponentially decreasing density at large distances. In later calculations, this problem was addressed in the HF [8] and TF [9] approaches in a so-called subtraction procedure, where the nucleus was studied by means of a thermodynamic potential calculated as the difference between the thermodynamic potentials for the nucleus in equilibrium with a surrounding gas and that for the gas alone. This has the desirable feature that asymptotically the nuclear plus gas density falls off smoothly to the gas density and the result is independent of the size of the box. The solution does not exactly correspond to that of an isolated nucleus; the subtracted grand potential contains a residual contribution due to the coupling of the liquid and gas parts. This contribution is, however, expected to be small.

To compensate for the tendency of the nucleons to leave the hot nucleus, a suitable external pressure has to be imposed [7,10] on the system to maintain thermodynamic equilibrium. This constraint appears somewhat artificial for the description of an isolated hot nucleus in the laboratory, but is more relevant in the astrophysical context where a nucleus embedded in a hot nucleon gas is a possible scenario. In this paper, we look for a solution of the density profile of this hot nucleus immersed in a nucleon gas at the same temperature, which supplies the necessary external pressure. Mechanical equilibrium is maintained from the equality of the pressure in the condensed phase (the nucleus) with the external pressure exerted by the gas phase, and chemical equilibrium is maintained from the equality of the average number of particles leaving the hot nucleus with the average number of particles entering it; i.e., the pressure and the chemical potential in the two phases are equal. Since each phase is a two-component phase of neutrons and protons, the chemical potentials of neutrons and protons in both the liquid and gas phase are equal separately.

With the above-mentioned thermodynamic equilibrium conditions, the density profiles of nuclei at different temperatures are calculated in a refined TF approximation scheme in this paper. Beyond a certain temperature, the equilibrium conditions, however, cannot be maintained. The nucleus is unstable, and can no longer exist as a bound system. This temperature is called the limiting temperature $T_{\rm lim}$. We explore this limit for different nuclear systems. For a particular temperature, density, and composition (neutron-proton ratio) of the nucleon gas, we find that only one nuclear isotope can coexist in equilibrium. The evolution of this equilibrium nuclear mass as a function of temperature, density, and composition of the nucleon gas is then calculated. From the cal-

*Permanent address: Department of Physics, University of Kalyani, West Bengal 741235, India.

culated nuclear densities at different temperatures, we further calculate the lifetime of nuclei against neutron evaporation and the nuclear level density parameter. Assuming that the scaling model holds, we also calculate nuclear incompressibilities as a function of temperature.

In Sec. II, we review the variational Thomas-Fermi equations with the new prescription. The expressions for the incompressibility of finite nuclei, the neutron evaporation time, the level density parameter, etc., are also given. Results from the calculations are presented in Sec. III and the concluding remarks are given in Sec. IV.

II. THEORETICAL FRAMEWORK

In the following, we give a brief outline of the procedure for determining the density profiles of hot nuclei in the TF approximation with a chosen realistic two-body effective interaction.

A. Effective interaction

The TF interaction energy density is calculated with a momentum- and density-dependent finite-range two-body effective interaction [11]. This interaction is of the Seyler-Blanchard type [12,13]. It is given by

$$v_{\rm eff}(r,p,\rho)=C_{l,u}[v_1(r,p)+v_2(r,\rho)], \tag{1}$$

$$v_1=-(1-p^2/b^2)f(\mathbf{r_1},\mathbf{r_2}),$$

$$v_2=d^2[\rho_1(r_1)+\rho_2(r_2)]^n f(\mathbf{r_1},\mathbf{r_2}), \tag{2}$$

with

$$f(\mathbf{r_1},\mathbf{r_2})=\frac{e^{-|\mathbf{r_1}-\mathbf{r_2}|/a}}{|\mathbf{r_1}-\mathbf{r_2}|/a}. \tag{3}$$

Here a is the spatial range and b the strength of repulsion in the momentum dependence of the interaction; $r=|\mathbf{r_1}-\mathbf{r_2}|$ is the relative coordinate, and $p=|\mathbf{p_1}-\mathbf{p_2}|$ is the relative momentum of the two interacting nucleons. The subscripts l and u in the strength C refer to like pair (n-n or p-p) or unlike pair (n-p) interaction, d and n are measures of the strength of density dependence, and ρ_1 and ρ_2 are the densities at the sites of the two nucleons. The five potential parameters C_l, C_u, a, b, and d for a fixed value of the density exponent n are determined by reproducing (i) the volume energy coefficient for symmetric nuclear matter ($a_v=-16.1$ MeV), (ii) saturation density of normal nuclear matter ($\rho_0=0.1533$ fm^{-3}), (iii) the volume asymmetry energy coefficient ($J=34$ MeV), (iv) the surface energy coefficient of symmetric nuclear matter ($a_S=18.01$ MeV), and (v) the energy dependence of the real part of the nucleon-nucleus optical potential ($dV_{\rm An}/dE=0.30$; $V_{\rm An}$ is the potential mentioned).

TABLE I. The parameters of the effective interaction (in MeV fm units).

C_l	C_u	a	b	d	n	K_∞
291.7	910.6	0.6199	928.2	0.879	1/6	238

The details of the procedure for determining these parameters are given in Ref. [13]. The parameter n is obtained by reproducing the giant monopole resonance (GMR) energies of a large number of nuclei employing the scaling model [14]. The parameter set of the interaction is given in Table I. We have tested that this interaction reproduces the ground state binding energies, charge rms radii, charge distributions, etc., very well for a host of nuclei from ^{16}O to very heavy systems. Moreover, it has been found that the properties of pure neutron matter calculated with this type of interaction are in good agreement [15] with those obtained from other sophisticated interactions.

B. Self-consistent density profile

The interaction energy density for a finite system with the interaction chosen is given by

$$\mathscr{E}_I(r)=\frac{2}{h^3}\sum_\tau\left[\frac{1}{h^3}\int\{v_1(|\mathbf{r}-\mathbf{r}'|,|\mathbf{p}-\mathbf{p}'|)+v_2(|\mathbf{r}-\mathbf{r}'|,\rho)\}\{C_l n_\tau(\mathbf{r}',\mathbf{p}')+C_u n_{-\tau}(\mathbf{r}',\mathbf{p}')\}n_\tau(\mathbf{r},\mathbf{p})\right]d\mathbf{r}'d\mathbf{p}d\mathbf{p}'. \tag{4}$$

Here v_1 and v_2 are the potential functions given by Eq. (2), τ is the isospin index, and $n_\tau(\mathbf{r},\mathbf{p})$ is the position-dependent occupation probability. The Coulomb interaction energy density is given by the sum of the direct and exchange terms. They are given by

$$\mathscr{E}_D(r)=e^2\pi\rho_p(r)\int dr'r'^2\rho_p(r')g(r,r'), \tag{5}$$

$$\mathscr{E}_{\rm ex}(r)=-\frac{3e^2}{4\pi}(3\pi^2)^{1/3}\rho_p^{4/3}(r). \tag{6}$$

Here $\rho_p(r)$ is the density profile of the protons and

$$g(r,r')=\frac{(r+r')-|r-r'|}{rr'}. \tag{7}$$

For one-component nuclear matter of constant density ρ_0 in equilibrium at temperature T under a constant pressure P, the self-consistent occupation probablity $n(\mathbf{p})$ is obtained by minimizing the thermodynamic potential

$$G = E - TS - \mu A + P\Omega, \tag{8}$$

where E and S are the total energy and entropy of the system, μ the chemical potential, and Ω the volume. Following Ref. [13], the minimization leads to the expression for occupation probability as

$$n(\mathbf{p}) = \left[1 + \exp\left\{\left(\frac{p^2}{2m} + V^0 + p^2 V^1 + V^2 - \mu + P/\rho_0\right)/T\right\}\right]^{-1}, \tag{9}$$

where m is the nucleon mass, V^2 a rearrangement potential term appearing because of the density dependence in the interaction given by Eq. (1), and $V^0 + p^2 V^1$ is the single-particle potential, the momentum-dependent part of which determines the effective nucleon mass defined as

$$m^* = \left[\frac{1}{m} + 2V^1\right]^{-1}. \tag{10}$$

For the two-component finite nuclear system, the occupation probability is position dependent, and in the local density approximation can be written as

$$n_\tau(\mathbf{r},\mathbf{p}) = \left[1 + \exp\left\{\left(\frac{p^2}{2m^*_\tau(r)} + V^0_\tau(r) + V^2_\tau(r) + \delta_{\tau,p} V_C(r) - \mu_\tau + P/\rho(r)\right)/T\right\}\right]^{-1}. \tag{11}$$

Here an extra term $V_C(r)$ enters because of the inclusion of Coulomb force. To arrive at Eq. (11), the zeroth order TF approximation has been used. The corrections to the kinetic energy density in the form of density gradient terms have not been included because of the following reasons. First, the potential parameters are determined using the zeroth order TF approximation. Second, the corrections which are mostly important in the density tail region are not yet physically well founded [16] and therefore have not been included in our calculations.

In Eq. (11),

$$V^0_\tau(r) = \int d\mathbf{r}'[v_2(|\mathbf{r}-\mathbf{r}'|,\rho) - f(\mathbf{r},\mathbf{r}')][C_l\rho_\tau(r') + C_u\rho_{-\tau}(r')] + \frac{4\pi}{b^2h^3}\int d\mathbf{r}' f(\mathbf{r},\mathbf{r}')$$
$$\times[C_l(2m^*_\tau(r')T)^{5/2}J_{3/2}(\eta_\tau(r')) + C_u(2m^*_{-\tau}(r')T)^{5/2}J_{3/2}(\eta_{-\tau}(r'))], \tag{12}$$

$$V^1_\tau(r) = \frac{1}{b^2}\int d\mathbf{r}' f(\mathbf{r},\mathbf{r}')[C_l\rho_\tau(r') + C_u\rho_{-\tau}(r')], \tag{13}$$

$$V^2_\tau(r) = \int d\mathbf{r}' \frac{\partial v_2}{\partial\rho(r')}\sum_{\tau'}[C_l\rho_{\tau'}(r) + C_u\rho_{-\tau'}(r)]\rho_{\tau'}(r'), \tag{14}$$

and the Coulomb single-particle potential is the sum of direct and exchange terms,

$$V_C(r) = e^2\pi\int dr' r'^2 \rho_p(r') g(r,r') - \frac{3e^2}{4\pi}(3\pi^2)^{1/3}\rho_p^{1/3}(r). \tag{15}$$

The density is obtained from

$$\rho_\tau(\mathbf{r}) = \frac{2}{h^3}\int n_\tau(\mathbf{r},\mathbf{p})d\mathbf{p}$$
$$= \frac{4\pi}{h^3}[2m^*_\tau(r)T]^{3/2}J_{1/2}(\eta_\tau(r)). \tag{16}$$

In Eqs. (12) and (16), $J_k(\eta)$'s are the Fermi integrals,

$$J_k(\eta) = \int_0^\infty \frac{x^k}{1+\exp(x-\eta)}dx \tag{17}$$

and

$$\eta_\tau(r) = [\mu_\tau - V^0_\tau(r) - V^2_\tau(r) - \delta_{\tau,p}V_C(r) - P/\rho(r)]/T. \tag{18}$$

The total entropy of the nucleus, in the Landau-quasiparticle approximation, is given by

$$S=\sum_{\tau}-\frac{2}{h^3}\int\{n_\tau(\mathbf{r},\mathbf{p})\ln n_\tau(\mathbf{r},\mathbf{p})+[1-n_\tau(\mathbf{r},\mathbf{p})]\ln[1-n_\tau(\mathbf{r},\mathbf{p})]\}d\mathbf{r}d\mathbf{p}, \tag{19}$$

which after momentum integration leads to

$$S=\int d\mathbf{r}\sum_{\tau}\rho_\tau(r)\left[\frac{5}{3}\frac{J_{3/2}(\eta_\tau(r))}{J_{1/2}(\eta_\tau(r))}-\eta_\tau(r)\right]. \tag{20}$$

To arrive at the self-consistent density profile at a given temperature T in equilibrium with the external gas at the same T the following sequence of steps is followed.

(i) To start with, we fix an external pressure P and choose guess densities for neutrons and protons given by Fermi functions normalized to the neutron and proton numbers of the nucleus.

(ii) The interaction $V_\tau^1(r)$ is calculated from Eq. (13) and then $m_\tau^*(r)$ is obtained from Eq. (10).

(iii) The fugacity $\eta_\tau(r)$ is calculated from Eq. (16).

(iv) The different components of the single-particle potentials $V_\tau^0(r)$, $V_\tau^2(r)$, and $V_C(r)$ are obtained from Eqs. (12), (14), and (15).

(v) The chemical potentials μ_τ's are obtained from the constraint of number conservation as [see Eq. (18)]

$$\mu_\tau=\frac{1}{A_\tau}\int d\mathbf{r}[T\eta_\tau(r)+V_\tau^0(r)+V_\tau^2(r)+\delta_{\tau,p}V_C(r)+P/\rho(r)]\rho_\tau(r), \tag{21}$$

where A_τ is the number of neutrons or protons.

(vi) The fugacity $\eta_\tau(r)$ is recalculated from Eq. (18) using μ_τ obtained in the previous step.

(vii) The density $\rho_\tau(r)$ is recalculated with this fugacity from Eq. (16) with the $m_\tau^*(r)$ obtained in step (ii).

Steps (i)–(vii) are then repeated until the chemical potentials and the densities obtained in the $(n-1)$th and nth iteration match the desired accuracy.

(viii) The above calculations for the densities are repeated for different values of P and thus one obtains the liquid lines [see Fig. 1(a)] for the neutrons and the protons in the nucleus in the P-μ plane.

(ix) To obtain the gas lines in the $P-\mu$ plane for a fixed neutron-proton asymmetry X_g in the infinite nucleon gas [defined as $X_g=(\rho_g^n-\rho_g^p)/\rho_g$, where ρ_g is the density of the gas, assumed to be neutral], the gas pressure and the chemical potentials μ_g^n and μ_g^p are obtained for different values of the gas density [13].

(x) The points of intersection of the liquid lines with the gas lines give $\mu_g^p(X_g)=\mu_l^p(X_g)$ and $\mu_g^n(X_g)=\mu_l^n(X_g)$ where the subscript l refers to the liquid phase (the nucleus), but the pressure $P_p(X_g)$ and $P_n(X_g)$ at the points of intersection are in general different as can be seen from Fig. 1(a).

(xi) The above steps are repeated for different values of X_g and the thermodynamically stable solution is obtained by finding out the intersection of $P_p(X_g)$ and $P_n(X_g)$, as shown in Fig. 1(b).

In passing, we may remark that the pressure term as introduced in Eq. (9) is extremely important in the description of multifragmentation of nuclei under compression in a quantum statistical model, which would be presented in a different context.

C. Incompressibility of a finite nucleus

The incompressibility of infinite symmetric nuclear matter at a finite temperature T is given by

$$K_\infty(T)=\left[9\rho^2\frac{\partial^2 f}{\partial\rho^2}\right]_{\rho=\rho_\infty(T)}, \tag{22}$$

where f is the free energy per particle of the matter and $\rho_\infty(T)$ is its saturation density at the temperature concerned. For a finite nucleus, the compression modulus is calculated in the scaling model [17] as

$$K_A(T)=\left[\lambda^2\frac{\partial^2[F(\lambda)/A]}{\partial\lambda^2}\right]_{\lambda\to1}, \tag{23}$$

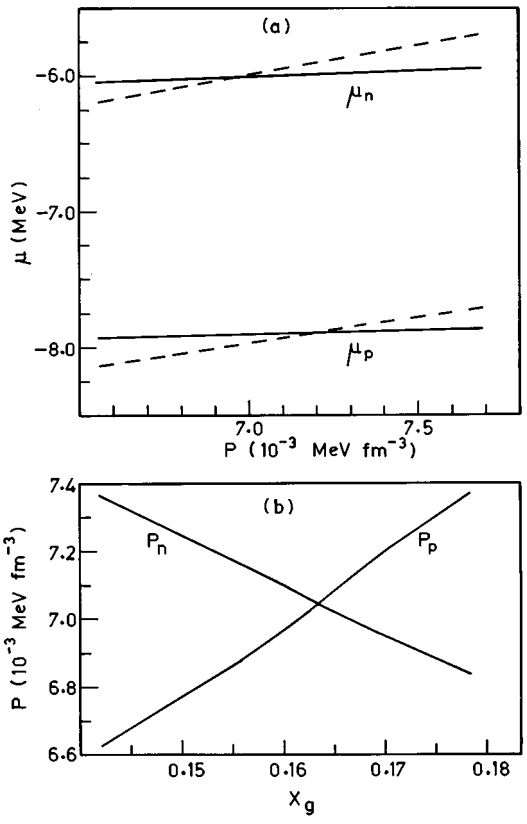

FIG. 1. (a) The P-μ curve for ^{208}Pb for $X_g=0.17$. The dashed lines correspond to the gas phase and the solid lines correspond to the liquid (nucleus) phase. The intersections of the liquid and gas lines define equilibrium μ_n and μ_p and thus also give corresponding equilibrium pressures P_n and P_p. (b) The variation of P_n and P_p with X_g is shown. Their intersection gives the equilibrium values of pressure and neutron-proton asymmetry X_g in the gas phase.

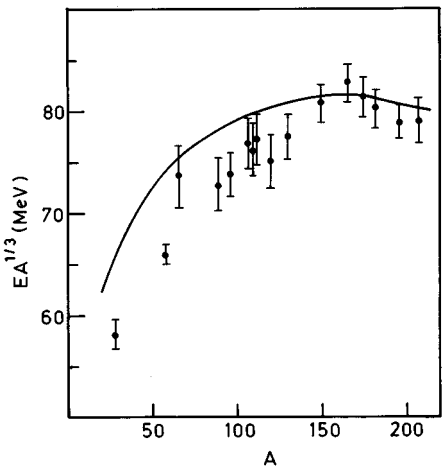

FIG. 2. The GMR energies plotted as a function of mass number. The points with error bars are the experimental energies [26].

where $F=E-TS$ is the total free energy of the nucleus and λ is the scaling parameter. Whenever the distance r is scaled as $r\rightarrow\lambda r$, the density $\rho(r)\rightarrow\lambda^3\rho(\lambda r)$. The single-particle occupations are not modified by scaling transformations [18]. With the help of Eqs. (4)–(7) and (20), the free energy of the nucleus can be easily evaluated once the densities are known from the variational procedure and then $K_A(T)$ is calculated. In the hydrodynamic model, the compression modulus of the nucleus is related to the GMR energy E_G as

$$E_G=\hbar\sqrt{\frac{K_A}{m\langle r^2\rangle}}, \tag{24}$$

where m is the nucleon mass and $\langle r^2\rangle$ is the mean square radius of the matter distribution. Here E_G, K_A, and $\langle r^2\rangle$ all refer to zero temperature. In the effective interaction given by Eqs. (1) and (2), the density exponent n is chosen such that the GMR energies in the heavy mass region (where the scaling model is expected to be valid) are fairly well reproduced. An optimal choice is given by $n=1/6$; the fit to the experimental data is displayed in Fig. 2.

D. Neutron evaporation time

In calculating the evaporation times from a hot nucleus, two different approaches are followed: (i) The nucleus is assumed to be in thermodynamic equilibrium with a surrounding nucleon gas and (ii) the nucleus is assumed to be isolated and thermodynamically unstable.

1. Nucleus in thermodynamic equilibrium

Assuming that the nucleus is in equilibrium with a surrounding gas of nucleons with neutron density ρ_g^n at temperature T, the number of neutrons evaporating from the nucleus would be equal to the number of neutrons entering it. The number of neutrons hitting (and subsequently getting absorbed) unit area of the nucleus with velocity $\mathbf{v}$ from the gas phase in unit time is

$$n_0=\frac{\rho_g^n\int d\mathbf{v}f(\mathbf{v})v\cos\theta\Theta(\pi/2-\theta)}{\int d\mathbf{v}f(\mathbf{v})}.$$

The step function Θ is introduced to take into account only those neutrons that are moving towards the surface. We then get

$$n_0=\frac{\rho_g^n}{4}\langle v\rangle. \tag{25}$$

Assuming Fermi-Dirac distribution for the gas,

$$\langle v\rangle=\sqrt{\frac{2T}{m}}\frac{J_1(\eta_n)}{J_{1/2}(\eta_n)}, \tag{26}$$

where η_n is given by Eq. (18) for the gas phase. In the limit of very low density, as $J_k(\eta)\sim\Gamma(k+1)e^{\eta}$, the velocity distribution reduces to the Boltzmann distribution and then

$$n_0\approx\frac{\rho_g^n}{4}\sqrt{\frac{8T}{\pi m}}. \tag{27}$$

The rate of neutrons hitting the nuclear surface area $4\pi R^2$ is $\mathcal{N}=4\pi R^2 n_0$ and then the evaporation time is given by

$$\tau=\frac{1}{\mathcal{N}}=\left[\rho_g^n R^2\sqrt{\frac{8\pi T}{m}}\right]^{-1}. \tag{28}$$

At very low density, $m^*\approx m$, $\eta\approx\mu/T$, and then using the expansion for $J_{1/2}(\eta)$ for the density as given by Eq. (16), we get, from Eq. (28),

$$\frac{1}{\tau}=\frac{2m}{\pi\hbar^3}(RT)^2e^{\mu_n/T}. \tag{29}$$

Here μ_n is the neutron chemical potential of both the gas and the nucleus, existing in thermodynamic equilibrium.

2. Metastable nucleus

For an isolated hot nucleus, the evaporation rate can also be calculated from the assumption that the nucleons move independently inside the nucleus in a single-particle potential of strength U_0 obeying Fermi-Dirac distribution, and when the energy associated with their radial motion is greater than U_0, they escape out of the surface. There the flux of neutrons emitted from the nucleus is given by

$$\mathcal{F}=2\pi\int_{U_0}^{\infty}f(\epsilon)d\epsilon\int_0^{\theta_{\max}}v\ \cos\theta\ \sin\theta\ d\theta\ \rho_n, \tag{30}$$

where $\cos\theta_{\max}=v_{\min}/v$ with $\frac{1}{2}mv_{\min}^2=U_0$ and

$$f(\epsilon)=\frac{3}{8\pi}\frac{1}{(\epsilon_{F_0})^{3/2}}\frac{\sqrt{\epsilon}}{e^{(\epsilon-\epsilon_F)/T}+1}. \tag{31}$$

Here ρ_n is the neutron density in the nucleus and ϵ_{F_0}, ϵ_F are the neutron Fermi energies at zero and finite temperature. The integral (30) can be evaluated to be

$$\mathcal{F}=\frac{3}{8}\sqrt{\frac{2}{m}}\frac{1}{(\epsilon_{F_0})^{3/2}}T^2\sum_{k=0}^{\infty}(-)^k\frac{(e^{\mu_n/T})^{k+1}}{(k+1)^2}\rho_n, \tag{32}$$

where $\mu_n=(\epsilon_F-U_0)$. With $\rho_n=(2m\epsilon_F/\hbar^2)^{3/2}/3\pi^2$, the evaporation time can be calculated from

$$\frac{1}{\tau}=4\pi R^2\mathscr{F}$$
$$=\left(\frac{\epsilon_F}{\epsilon_{F_0}}\right)^{3/2}\frac{2mR^2T^2}{\pi\hbar^3}\sum_{k=0}^{\infty}(-)^k\frac{(e^{\mu_n/T})^{k+1}}{(k+1)^2}. \quad (33)$$

For not too high temperatures $\epsilon_F\approx\epsilon_{F_0}$, the series is highly convergent, and then taking only the first term

$$\frac{1}{\tau}=\frac{2m}{\pi\hbar^3}(RT)^2e^{\mu_n/T}, \quad (34)$$

an expression that agrees exactly with that given in Eq. (29) and with that given in Refs. [4] and [19] though obtained from a different physical premise. The choice of the chemical potential is ambiguous for an isolated hot nucleus. In the absence of any better prescription, we choose the chemical potential obtained from phase-equilibrium conditions.

E. Level density parameter

Many average nuclear properties of not too hot nuclei ($T\leqslant 4$ MeV) may be nearly temperature independent when at least no instability is involved, such as in the case of giant resonances [18]. One interesting output of our calculation is hence to estimate an upper limit below which the bulk nuclear properties may not be affected too drastically by finite temperature effects. One such example is the level density parameter a entering in Bethe's formula for calculating the density of states of an excited nucleus $\rho(A,\epsilon^*)$ [20]:

$$\rho(A,\epsilon^*)=\frac{1}{12}\left(\frac{\pi^2}{a}\right)^{1/4}\epsilon^{*-5/4}\exp(2\sqrt{a\epsilon^*}). \quad (35)$$

In arriving at this formula, it is assumed that the nucleus is at zero temperature while the statistics over its spectrum is performed at finite temperature. This formula therefore has validity provided the level density parameter a is not too sensitive to temperature. In earlier Hartree-Fock calculations [19] or in semiclassical studies in the subtraction procedure [9,21] with zero-range Skyrme interaction, it is already found that for $T\leqslant 4$ MeV, a is nearly temperature independent; in our prescription with a finite range interaction, it may be interesting to find out the range of validity of the assumption.

The single-particle level density $g_\tau(\epsilon)$ for neutrons and protons is given by [21]

$$g_\tau(\epsilon)=\frac{\sqrt{2}}{\pi^2\hbar^3}\int d\mathbf{r}m_\tau^{*3/2}(r)\sqrt{\epsilon-V_\tau^0(r)}, \quad (36)$$

where V_τ^0 is given by Eq. (12). The level density parameter is given by $a=\Sigma_\tau a_\tau$ where $a_\tau=\pi^2/6g_\tau(\epsilon=\epsilon_F)$, and then in the local density approximation, it can be written as

$$a=\frac{(3\pi^2)^{1/3}}{6\hbar^2}\int d\mathbf{r}\sum_\tau\,[m_\tau^*(r)\rho_\tau^{1/3}(r)], \quad (37)$$

where $\rho_\tau(r)$ are the nuclear densities calculated from the variational procedure.

III. RESULTS AND DISCUSSIONS

The parameters of the effective interaction given by Eqs. (1)–(3) are determined (for a fixed value of the density exponent n in the interaction) by reproducing the volume energy per particle of symmetric nuclear matter, its saturation density, volume asymmetry energy, surface energy, and the energy dependence of the real part of the nucleon-nucleus optical potential. The details of the procedure for the determination of these parameters are given in Ref. [13]. The density exponent n is varied until a fairly well reproduction of the GMR energies in relatively heavier nuclei is achieved (see Fig. 2). The parameters so obtained for the effective interaction are given in Table I. The incompressibility of symmetric nuclear matter obtained from this interaction is $K_\infty=238$ MeV, close to the value of $K_\infty=210\pm 30$ MeV obtained from an extended analysis by Blaizot [22].

Once the interaction is chosen, self-consistent density solutions are obtained at different temperatures for a number of nuclei immersed in an external nucleon gas. The calculations range over the whole periodic table (excluding the very light nuclei) near the β-stability line. For extremely small temperature T ($\sim$0.1 MeV), one expects the external gas pressure to be nearly zero. We thus obtain the density which is indistinguishable from the zero temperature solution. In absence of an external pressure, at finite temperature, from Eq. (18) one expects η to go over to μ/T at large distances, and then from Eq. (16), one finds ρ to be nonvanishing there. Thus the nuclear density profile becomes unphysical depending on the size of the box in which the calculations are done. With the inclusion of the pressure term, the density falls off smoothly to zero at a finite distance and the results are independent of the box size.

In Fig. 1, we tentatively show for a representative system, namely, ^{208}Pb, how to obtain the equilibrium density solutions for the nuclear liquid (^{208}Pb) maintaining both mechanical and chemical equilibrium with the external gas comprising of protons and neutrons. In the top panel of the figure, the solid lines show the variation of the neutron and proton chemical potentials in the liquid phase (nucleus) with external pressure P (equated to be the pressure of the external gas) for a fixed neutron-proton asymmetry X_g for the nucleon gas and the dashed lines correspond to those for the neutron and proton gas. The intersections of the neutron liquid-gas lines and the proton liquid-gas lines show that chemical equilibria for the liquid-gas phases for both neutron and proton are achieved, but the equilibrium pressures (designated by P_n and P_p) are different. In the bottom panel, it is shown that these equilibrium pressures intersect when plotted as a function of X_g. This intersection point gives the value of the pressure required for thermodynamic liquid-gas phase equilibrium exerted by the external nucleon gas of asymmetry X_g (given by the intersection point). This also gives the density of the nucleon gas ρ_g and since X_g is known ρ_g^n and ρ_g^p are determined.

In Fig. 3, the variations of the gas density (top panel) and the corresponding gas pressure (bottom panel) are displayed as a function of temperature for the stability of two represen-

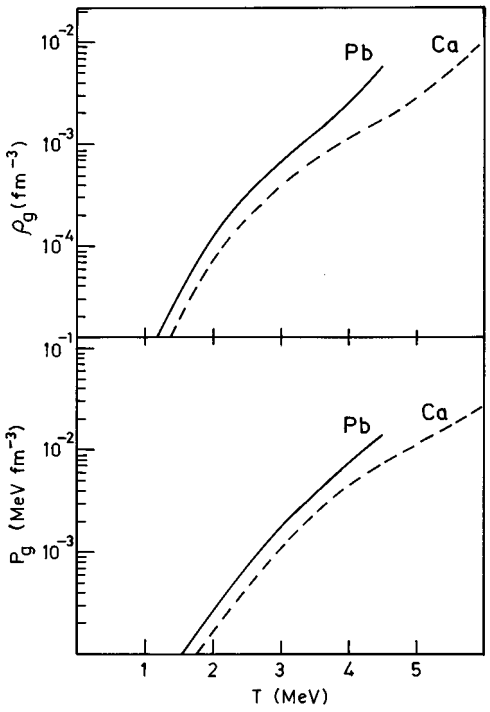

FIG. 3. The equilibrium gas density and gas pressure as a function of temperature shown for two systems ^{40}Ca and ^{208}Pb.

tative systems ^{40}Ca and ^{208} Pb. They extend up to the limiting temperature $T_{\rm lim}$ beyond which the thermodynamic equilibrium conditions can no longer be satisfied. At low temperature, both the gas pressure and density are very small; they increase almost exponentially with increasing temperature. The gas density reaches a value of $\sim 5-10$ % (depending on the system) of the nuclear interior density at the limiting temperature. For the lighter nucleus, at the same temperature, the gas density is usually smaller. It is also found that (see Fig. 7), whereas for ^{40}Ca the gas is extremely proton rich, for ^{208}Pb the neutron concentration is higher. This is consistent with the fact that in ^{40}Ca the neutrons are comparatively more tightly bound, whereas in ^{208}Pb the protons have more separation energy than the neutrons. If the Coulomb effects in the gas phase were considered, one expects the proton concentration (ρ_g^p) there to be lower.

In Fig. 4, the proton density distribution for ^{150}Sm is shown at zero temperature and also at $T=5$ MeV corresponding to its limiting temperature. As expected, with increase in temperature, the central density is reduced and the surface becomes more diffuse, but these effects as obtained here are less pronounced compared to those of previous calculations [23,24]. In Fig. 5, the variation with temperature of the sharp-surface radius constant r_0 is displayed for the systems ^{40}Ca, ^{90}Zr, and ^{208}Pb. This radius constant is related to the mean square radius $\langle r^2\rangle$ by $r_0A^{1/3}=\sqrt{5/3}\langle r^2\rangle^{1/2}$. The radius increases nearly quadratically up to a temperature close to the limiting temperature as $r_0(T)\approx r_0(0)(1+\alpha T^2)$. However, near the limiting temperature, the radius shows a plateau. This is due to a delicate interplay between the thermal motion trying to diffuse the nuclear tail and the external pressure trying to compress it. In previous calculations [23,24], the expansion coefficient α is found to be $\alpha\approx 0.001$; in our

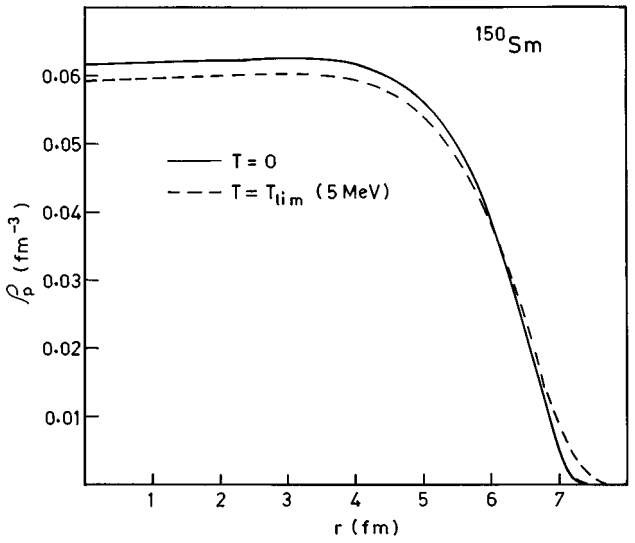

FIG. 4. The charge density distributions for ^{150}Sm at $T=0$ and at the limiting temperature $T_{\rm lim}=5$ MeV.

calculation, it turns out to be ≈ 0.0007.

In Fig. 6, the limiting temperature $T_{\rm lim}$ is shown as a function of mass of the nucleus on the β-stability line. With increasing mass, the limiting temperature decreases due to Coulomb effects. The values of the limiting temperatures are consistent with the maximum excitation energy that can be deposited [1] in finite nuclei in nuclear collisions. In Fig. 7, the equilibrium nuclear masses on the β-stability line are displayed as a function of neutron and proton gas densities at different temperatures. At a fixed temperature, it is found that the density of the neutron gas increases monotonically with mass number to maintain thermodynamic equilibrium. The density of the proton gas on the other hand shows a minimum around $A\approx 120-130$. This variation of the neutron and proton gas densities with mass number is intimately related

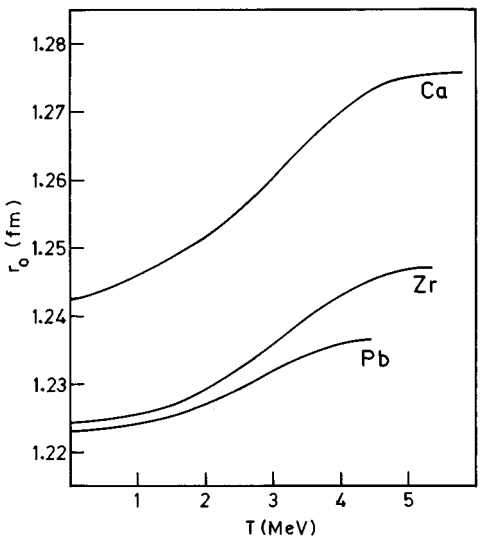

FIG. 5. The radius constant r_0 as a function of temperature for the systems ^{40}Ca, ^{90}Zr, and ^{208}Pb. It is related to the mean square radius as $r_0A^{1/3}=\sqrt{5/3}\langle r^2\rangle^{1/2}$.

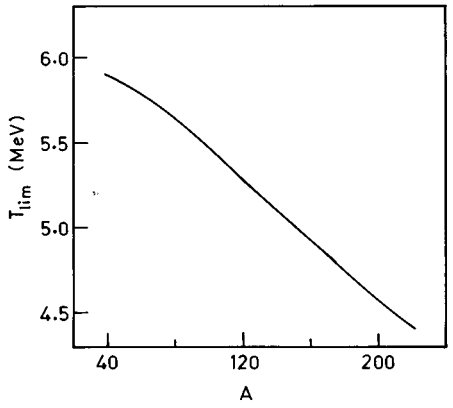

FIG. 6. The limiting temperature $T_{\rm lim}$ as a function of mass number.

to the behavior of the neutron and proton separation energies with increasing mass. Exploiting the condition for thermodynamic equilibrium, from Eq. (16) for low gas densities we find that $\rho_g \sim e^{\mu/T}$, where μ is negative of the nucleon separation energy. If the neutrons (protons) are more bound, the corresponding neutron (proton) gas density is therefore low. In our model calculations in the TF framework, it is found that the neutron separation energy decreases with mass number whereas the proton separation energy shows a maximum at $A \approx 120-130$. A similar behavior for the separation energies is also observed in the liquid-drop model. This explains

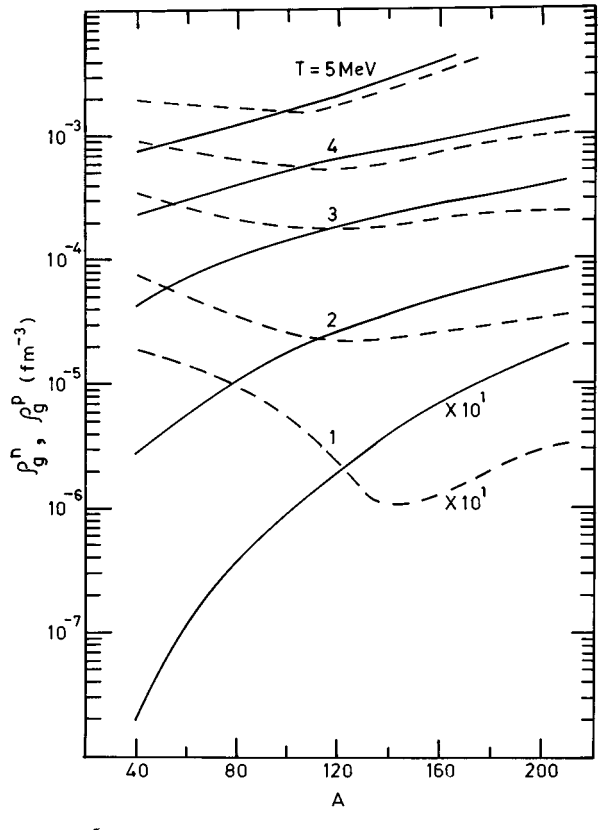

FIG. 7. The equilibrium neutron (solid lines) and proton (dashed lines) gas densities for different masses on the β-stability line at different temperatures.

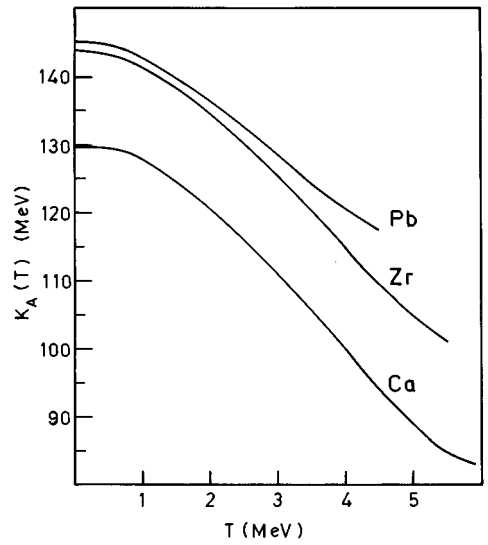

FIG. 8. The temperature dependence of compression modulii K_A of the nuclei ^{40}Ca, ^{90}Zr, and ^{208}Pb.

the behavior of the neutron and proton gas density with mass number. As the temperature is raised, the equilibrium gas densities increase. Since the chemical potential is weakly dependent on temperature compared to $1/T$, the increase in the gas density with temperature is understood. The relation $\rho_g \sim e^{\mu/T}$ also explains the weak dependence of the gas density with mass number with increase in temperature. From the figure it is also found that for a fixed neutron-proton asymmetry and a given gas density, only one nucleus can remain in stable equilibrium with a specific charge and mass. This finding might have an important bearing in nucleosynthesis in the astrophysical context. However, the situation becomes more complicated there due to the presence of electrons.

In Fig. 8, the temperature dependences of the compression modulus of both light, medium-heavy, and heavy systems are displayed. The decrease with temperature is given approximately by $K_A(T) \sim K_A(0)(1-\delta T^2)$ where $\delta \sim 0.012-0.014$, depending on the system, being higher for lighter nuclei. This temperature dependence is $\sim$ 3 times larger compared to that for symmetric infinite nuclear matter [13] and is in conformity with that obtained in a recent calculation [25] using the Skyrme force, SKM*. The strong temperature dependence of the surface free energy is the origin of this sharper decline in $K_A(T)$ compared to $K_\infty(T)$.

In Fig. 9, the level density parameter $a(T)$ given by the Eq. (37) is plotted as a function of temperature for four nuclei ^{40}Ca, ^{90}Zr, ^{150}Sm, and ^{208}Pb. The level density parameter increases slowly at low temperatures and then falls down a little near the limiting temperature. The fractional increase is most prominent for lighter nuclei ($\sim$10% for ^{40}Ca, $\sim$5% for ^{208}Pb). This temperature dependence is a little stronger than that obtained by Suraud *et al.* [21] where a 2% increase is reported. Near the limiting temperature, there is a striking difference in the behavior of the level density parameter. Whereas in Ref. [21], $a(T)$ increases rather sharply near $T_{\rm lim}$, in our calculation, $a(T)$ decreases, presumably because of the compressional effects introduced by the external gas on the density tail. It may be further noted that the values of

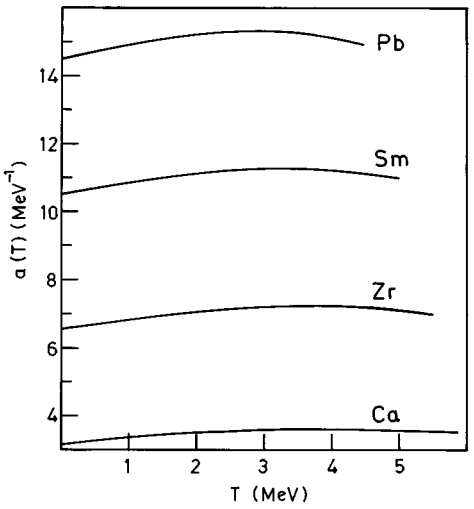

FIG. 9. The temperature dependence of the level density parameter a for ^{40}Ca, ^{90}Zr, ^{150}Sm, and ^{208}Pb.

$a(T)$ obtained in our calculation are $\sim$15% smaller compared to those obtained in Ref. [21] where the SKM force is used.

The level density parameter is intimately connected with the entropy of the system by $S \approx 2a(T)T$. In Fig. 10, we plot the entropy per particle as a function of temperature for a light (Ca) and a heavy (Pb) nucleus from this approximate relation (dashed line) and compare them with the values (solid line) obtained from the Landau-quasiparticle approximation given by Eq. (20). We also show (dotted line) the entropy per particle for infinite symmetric nuclear matter at different temperatures. The entropy increases almost linearly with temperature. It is found that except at very low temperatures, the approximate values are always larger. It is also seen that at the same temperature, lighter nuclei generate more entropy per particle. This is consistent with the fact that

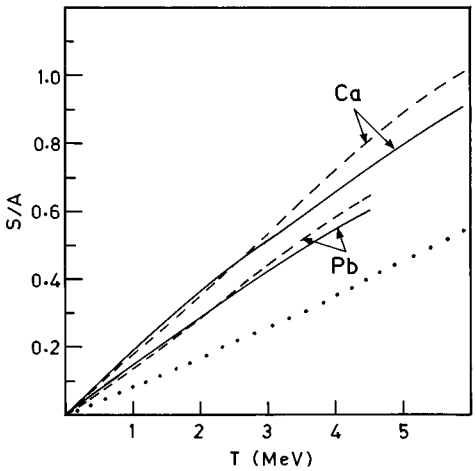

FIG. 10. The dotted line shows the entropy per particle for symmetric infinite nuclear matter. The solid lines correspond to entropy per particle for ^{40}Ca and ^{208}Pb (as marked) calculated from Eq. (20). The dashed lines are the corresponding approximate values given by $2a(T)T$.

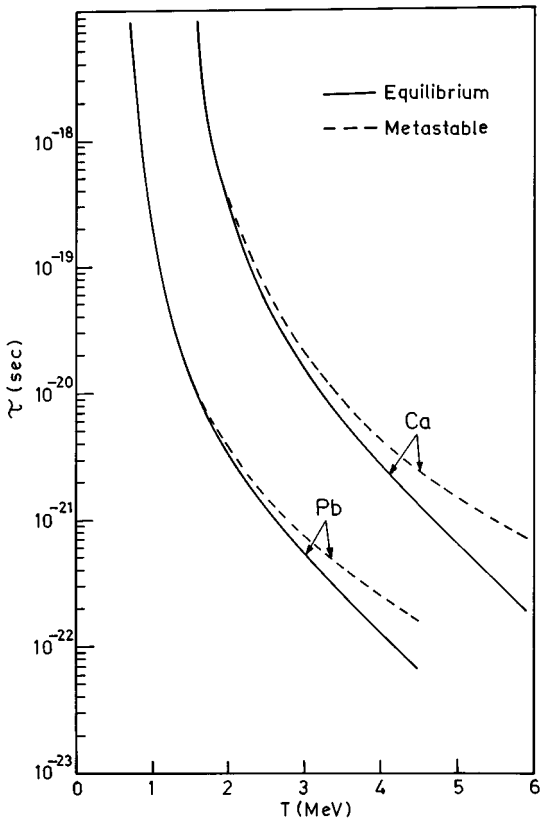

FIG. 11. Lifetime against neutron evaporation as a function of temperature for ^{40}Ca and ^{208}Pb, evaluated for metastable situation and for liquid-gas phase equilibrium.

$a(T)/A$ is larger for lighter nuclei as can be seen from Fig. 9.

The evaporation times for neutrons are calculated for the same set of nuclei as in Fig. 10 at different temperatures in the models of both metastable and thermodynamic equilibria and are displayed in Fig. 11. At low temperatures, the evaporation times calculated from both the models for a particular nucleus are the same; at higher temperatures, the model for thermodynamic equilibrium yields evaporation times that are consistently lower. This means that hot nuclei in the metastable description are comparatively more stable against neutron evaporation. This is counterintuitive; in equilibrium calculations, since the external gas exerts a pressure on the nucleus, one expects it to be more stable than under zero pressure conditions as in the metastable situation. However, in the metastable situation, the choice of the chemical potential that enters in Eq. (33) is ambiguous. The chemical potential in the equilibrium situation is therefore used for the calculation of the lifetimes in the metastable description. This may be the possible reason for the longer lifetime obtained in the metastable situation.

IV. SUMMARY AND CONCLUSIONS

We have proposed a prescription to solve self-consistently the density profile of two-component hot nuclei in thermodynamic equilibrium with a surrounding gas in a refined Thomas-Fermi approximation. The effective interaction employed is momentum and density dependent and of finite range, the parameters of which are chosen such that the bulk

properties of finite nuclei as well as the collective GMR energies are quite well reproduced. The incompressibility of symmetric nuclear matter then turns out to be $K_\infty = 238$ MeV, in close agreement with values obtained from more detailed calculations [22]. The density solutions for hot nuclei obtained in this prescription are found to be independent of the box size in which the calculations are done. For stability of systems, it is found that the hotter the nuclei, the larger is the pressure or equivalently the density of the surrounding gas. At a fixed temperature, the density of the neutron gas increases monotonically with mass number whereas the density of the proton gas shows a minimum at $A \sim 120-130$, in close parallel with the observed behavior of neutron and proton separation energies with mass number in the liquid-drop model. It further follows from the calculation that at a fixed temperature, in an external surrounding gas (of specific density and neutron-proton asymmetry), only one nucleus can remain immersed in stable equilibrium with a particular charge and mass. Increasing the temperature would entail a change in the density and composition of the external gas until the chemical and mechanical equilibrium between the nucleus and surrounding gas are lost at the limiting temperature. The calculated limiting temperatures are consistent with the highest possible excitation energies deposited in different nuclear systems in energetic nuclear collisions. As the temperature increases, the nucleus expands, but the expansion of the nuclear radius seems to be a little slower compared to previous calculations [4,23,24], particularly near the limiting temperature. As a result, the temperature dependence of GMR energies is mostly governed by the temperature dependence of the compression modulus of finite nuclei and is given approximately by $E_G(T) \approx E_G(0)[1-0.007T^2]$, which is weak and consistent with calculations [25] as reported recently.

[1] D. Guerreau, in *Towards a Unified Picture of Nuclear Dynamics*, edited by Y. Abe, F. Sakata, and S. M. Lee, AIP Conf. Proc. No. 250 (AIP, New York, 1992), p. 347, and references therein.

[2] R. Balian, *Mécanique Statistique* (Ellipses, Paris, 1984).

[3] W. Stocker and J. Burzlaff, Nucl. Phys. **A202**, 265 (1973).

[4] A.H. Blin and M. Brack, Nucl. Phys. **A504**, 300 (1989).

[5] M. Brack and P. Quentin, Phys. Scr. A **10**, 163 (1974).

[6] M. Barranco and J. Treiner, Nucl. Phys. **A351**, 269 (1981).

[7] M. Brack, C. Guet, and H.B. Hakansson, Phys. Rep. **123**, 275 (1985).

[8] P. Bonche, S. Levit, and D. Vautherin, Nucl. Phys. **A436**, 265 (1985).

[9] E. Suraud, Nucl. Phys. **A462**, 109 (1987).

[10] J. Bartel, M. Brack, and M. Durand, Nucl. Phys. **A445**, 263 (1985).

[11] D. Bandyopadhyay and S.K. Samaddar, Nucl. Phys. **A484**, 315 (1988).

[12] R.G. Seyler and C.H. Blanchard, Phys. Rev. **124**, 227 (1961); **131**, 355 (1963).

[13] D. Bandyopadhyay, C. Samanta, S.K. Samaddar, and J.N. De, Nucl. Phys. **A511**, 1 (1990).

[14] M.M. Majumdar, S.K. Samaddar, N. Rudra, and J.N. De, Phys. Rev. C **49**, 541 (1994).

[15] N. Rudra and J.N. De, Nucl. Phys. **A545**, 608 (1992).

[16] W.D. Myers and W.J. Swiatecki, Ann. Phys. (N.Y.) **204**, 401 (1990).

[17] B.K. Jennings and A.D. Jackson, Nucl. Phys. **A342**, 23 (1980).

[18] M. Barranco, A. Polls, and J. Martorell, Nucl. Phys. **A444**, 445 (1985).

[19] P. Bonche, S. Levit, and D. Vautherin, Nucl. Phys. **A427**, 278 (1984).

[20] H.A. Bethe, Rev. Mod. Phys. **9**, 53 (1937).

[21] E. Suraud, P. Schuck, and R.W. Hasse, Phys. Lett. B **164**, 212 (1985).

[22] J.P. Blaizot, Phys. Rep. **64**, 171 (1980).

[23] R. Hasse and W. Stocker, Phys. Lett. **44B**, 26 (1973).

[24] X. Campi and S. Stringari, Z. Phys. A **309**, 239 (1983).

[25] P. Gleissl, M. Brack, J. Meyer, and P. Quentin, Ann. Phys. (N.Y.) **197**, 204 (1990).

[26] S. Shlomo and D.H. Youngblood, Phys. Rev. C **47**, 529 (1993).